ACADEMIC PRESS

Available online at www.sciencedirect.com

SCIENCE DIRECT®

Journal of Sound and Vibration 267 (2003) 1085–1106

JOURNAL OF SOUND AND VIBRATION

www.elsevier.com/locate/jsvi

Dynamic behaviour of structures in large frequency range by continuous element methods

J.B. Casimir*, T. Vinh, C. Duforêt

Laboratory of Structures and Rheology I.S.M.C.M. 3, rue Fernand Hainaut, 93407 Saint-OUEN, France

Received 26 July 2001; accepted 29 October 2002

Abstract

The continuous element method is presented in the context of the harmonic response of beam assemblies. A general formulation is described from the displacement solution of the elementary problem. A direct computation of elementary dynamic stiffness matrices is presented. In the present formulation, distributed loadings are taken into account. In the case of more complex geometries for which many coupling phenomena occur, an explicit formulation is no more conceivable. In this case, a numerical approach is presented. This approach allows an algorithmic computation of exact dynamic stiffness matrices. This method, called ''Numerical Continuous Element'', allows one to consider the coupled vibrations of curved beams and those of helical beams. The validation of this numerical method is achieved by comparisons with the harmonic response of various beams obtained by a finite element approach. Finally, a comparison between eigenfrequencies obtained experimentally and numerically for a straight beam and a helical beam has been made to evaluate the performances of the method.

1. Introduction

The two most popular computational methods used in structural dynamics are: the finite element method (FEM) and the boundary element method (BEM). While investigating higher frequency ranges for acoustic applications and using finite elements, structures are decomposed into smaller and smaller elements. The mesh size is chosen so that its largest dimension does not exceed the wavelength of the vibration. Going in this direction, when dealing with complex and large structures, the number of elements often becomes prohibitive. The calculation of eigenvalues in the range of medium frequency becomes cumbersome and time consuming. The BEM is

*Corresponding author. Fax: +149-4529-69.
E-mail address: casimir@ismcm-cesti.fr (J.B. Casimir).

0022-460X/03/$ - see front matter
doi:10.1016/S0022-460X(02)01533-X

generally used to study the acoustic radiation of structures. Green's formula permits one to bring the wave equation of the domain to its boundaries and the meshing of the structure concerns only its contour.

The continuous element method (CEM) constitutes a third class of methods, which have been the focus of attention of many researchers in Europe since 1975, particularly in aeronautical and naval engineering. Continuous element-based computer codes were elaborated in Sweden [1], France [2], the UK [3,4] and Germany [5]. For submarine structures, the CEM finds its application in the acoustical frequency range. This method has given rise to active research, see Refs. [6–8].

The CEM finds its theoretical foundations in elastodynamics. In direct line, it can be related to the Dynamic Stiffness Method using the characteristic functions of beams ([9–11]). Elementary or refined theories which take into account many effects (inertia, shear, warping, etc.) for beams as well as for plates and shells can be used. In the framework of an elastodynamic theory and with a given set of boundary conditions, it is possible, for a simple, element geometry (for example, rectangular or triangular plate), to obtain the exact solution of the vibration problem. This solution is not limited to lower frequency. Eigenfunctions are expressed as a combination of exponential functions (or trigonometric and hyperbolic functions) which are capable of describing an infinity of modes. In the case of plates, infinite series are adopted [7]. In practice, the series is truncated and the accuracy depends on the number of terms retained [12].

In a beam assembly, the dynamic stiffness matrix $[\mathbf{K}(\omega)]$ of each beam depends on the circular frequency ω. This matrix includes stiffness, mass and damping contributions.

$$[\mathbf{K}(\omega)]\mathbf{X}_e = \mathbf{F}_e, \tag{1}$$

where $\mathbf{X}_e$ is the displacement vector at both ends and $\mathbf{F}_e$ the generalized force vector at the same ends.

$[\mathbf{K}(\omega)]$ is determined by using beam characteristic functions. Coupling phenomena, as well as warping [13], can be taken into account in the equations of motion. They raise the order of these equations from 4 to 6 (or 8 or higher).

The solution of vibration problems concerning elements with simple known geometry, a matrix formulation defining displacement–force relationship permits solution of an assembly of beams. Fine meshing of the structure and decomposition of each beam into smaller elements is not necessary. This constitutes one of the main differences between finite elements and continuous elements. Fig. 1 represents the propulsion system cradle of a submarine in which the number of nodes is limited to 100 [14].

To solve this problem in the same frequency range, the number of nodes adopted for finite elements is several thousands.

The main difficulty is that the eigenvalue problem related to CE is non-linear [15] as opposed to that of the FEM, which is linear relative to ω^2. However, this method is very efficient to study the harmonic response of large structures.

This paper is devoted to beam assemblies. In the first part, the equations of motion for planar and non-planar beams are presented. In the simple case where various motions (extention, bending and torsion) are uncoupled, a close form expression of the dynamic stiffness matrix using characteristic functions is presented. When coupling motions are taken into account, a close form expression using characteristic functions becomes cumbersome, if not intractable. In these cases,

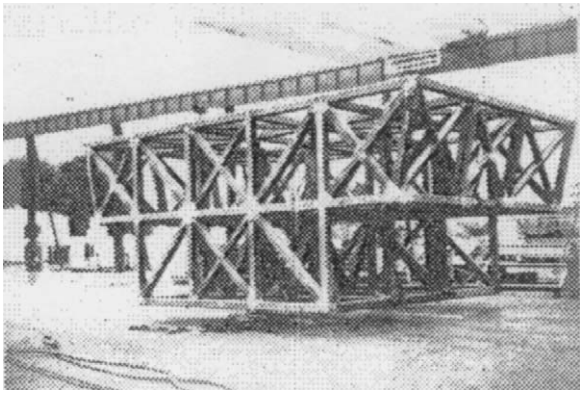

Fig. 1. Propulsion system cradle.

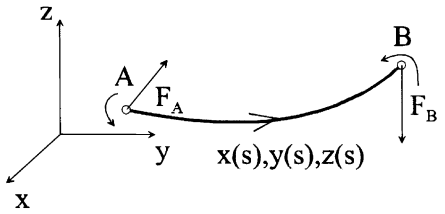

Fig. 2. Beam element.

an entirely numerical solution is proposed. This solution is not an approximation. For curved and non-planar beam, curvilinear co-ordinates are particularly appropriate. When curvature and tortuosity are constant along the middle line (helical beams), a restricted number of elements is adopted and can be reduced to one element, whereas the FEM requires atleast 50 elements or more for the same geometry.

The second part is devoted to numerical computation of frequency responses. Experimental validation and comparison with FEM computations are also presented.

2. Continuous element formulations

2.1. Equilibrium equations and force–displacement relationship

Let $L_{s,t}(\mathbf{u}, \mathbf{f})$ be a differential operator applied to the displacement vector $\mathbf{u}$ and the internal force vector $\mathbf{f}$ along the beam, Fig. 2.

$$
\begin{aligned}
&s \in [0,\ L],\ t > 0,\\
&L_{s,\,t}(\mathbf{u},\ \mathbf{f}) = q(s,\ t),\\
&\mathbf{f}(0,\ t) = -\mathbf{F}_A(t),\\
&\mathbf{f}(L,\ t) = \mathbf{F}_B(t),
\end{aligned}
\tag{2}
$$

where s is the curvilinear abscissa variable, t the time variable and $\mathbf{q}(s, t)$ the distributed loads along the beam.

Eqs. (2) represents the formulation of the elementary problem in which the operator $L_{s,t}$ is classified into two categories: the equilibrium equations and force–displacement relationship. To Eqs. (2), initial conditions have to be added.

For example, operator $L_{s,t}(\mathbf{u}, \mathbf{f})$ relative to a Timoshenko straight beam is of first order relative to abscissa s and second order relative to time t. It is given by the following expression:

$$\begin{aligned}
&\frac{\partial U_Y}{\partial s} - \frac{k_Y}{GS} F_Y - \Omega_Z = 0,\\
&\frac{\partial \Omega_Z}{\partial s} - \frac{M_Y}{EI_Z} = 0,\\
&\rho S \frac{\partial^2 U_Y}{\partial t^2} - \frac{\partial F_Y}{\partial s} = p_Y(s, t),\\
&\rho I_0 \frac{\partial^2 \Omega_Z}{\partial t^2} - \frac{\partial M_Z}{\partial s} - F_Y = m_Z(s, t),
\end{aligned} \tag{3}$$

where U_Y is the vertical translation and Ω_Z is the rotation of the section. S, k_Y, I_Z and I_0 are, respectively, the cross-sectional area, the Timoshenko shear deflection constant, the area and polar moments of inertia. E, G and ρ are, respectively, Young's modulus, the Coulomb modulus and the mass density. F_Y and M_Z are the internal shearing force and bending moment, p_Y and m_z are the distributed external vertical force and external bending moment.

In the particular case of harmonic regimes, the solution of Eqs. (2) is possible by removing the time variable t. This leads to a differential system where circular frequency ω appears as a parameter.

$$\begin{aligned}
s &\in [0, L],\\
L_{s,\omega}(\mathbf{u}, \mathbf{f}) &= q_\omega(s),\\
\mathbf{f}_\omega(0) &= -\mathbf{F}_A,\\
\mathbf{f}_\omega(L) &= \mathbf{F}_B.
\end{aligned} \tag{4}$$

Vector $\mathbf{E}(s) = [\mathbf{u}(s), \mathbf{f}(s)]$ is known as the state vector. Its components are the primary unknowns of the problem and depend on circular frequency ω.

2.2. Explicit continuous elements (ECE) and dynamic stiffness matrix

In the case of the general Timoshenko/Saint-Venant beam, the state vector has 12 components. From Eqs. (4), it is always possible to extract the differential equation satisfied by each component. In the more general case, these equations are 12th order ones.

In the case where the absence of coupling reduces the order of the equation of motion, explicit displacement solutions are tractable.

The explicit solutions of the equations relative to displacement components, that is to say the equations of motion, are obtained for the cases where the absence of coupling permits a reduction in equation order: displacement vector $\mathbf{u}$ is then expressed with characteristic functions.

$$\mathbf{u}(s, \omega) = [\mathbf{g}(s, \omega)]\mathbf{c} + \mathbf{g}_0(s, \omega), \tag{5}$$

where c is the vector whose components are 12 integration constants, $[\mathbf{g}(s,\omega)]$:(6×12) matrix consisting of characteristic functions which are solutions of the homogeneous equations of motion and $\mathbf{g}_0(s,\omega)$ the particular solutions of the equations of motion.

Displacements at both end $s=0$, $s=L$ give:

$$\mathbf{U}=\begin{pmatrix}\mathbf{u}(0,\omega)\\ \mathbf{u}(L,\omega)\end{pmatrix}=\begin{pmatrix}\mathbf{U}_A\\ \mathbf{U}_B\end{pmatrix}=\begin{pmatrix}[\mathbf{g}(0,\omega)]\\ [\mathbf{g}(L,\omega)]\end{pmatrix}\mathbf{c}+\begin{pmatrix}\mathbf{g}_0(0,\omega)\\ \mathbf{g}_0(L,\omega)\end{pmatrix}. \tag{6}$$

Integration constants obtained from the inversion of Eq. (6) are replaced in Eq. (5).

$$\mathbf{c}=\begin{pmatrix}[\mathrm{g}(0,\omega)]\\ [\mathrm{g}(L,\omega)]\end{pmatrix}^{-1}\begin{pmatrix}\mathbf{U}_A-\mathbf{g}_0(0,\omega)\\ \mathbf{U}_B-\mathbf{g}_0(L,\omega)\end{pmatrix}. \tag{7}$$

The displacement field along the beam is evaluated from the nodal displacement vector $\mathbf{U}=(\mathbf{U}_A,\mathbf{U}_B)^{\mathrm{T}}$. This leads to the following solution:

$$\mathbf{u}(s,\omega)=[\mathbf{g}(s,\omega)]\begin{pmatrix}[\mathbf{g}(0,\omega)]\\ [\mathbf{g}(L,\omega)]\end{pmatrix}^{-1}\begin{pmatrix}\mathbf{U}_A-\mathbf{g}_0(0,\omega)\\ \mathbf{U}_B-\mathbf{g}_0(L,\omega)\end{pmatrix}+\mathbf{g}_0(s,\omega). \tag{8}$$

Internal force unknowns $\mathbf{f}$ are deducted from the force–displacement relationship which are extracted from Eqs. (4):

$$\mathbf{f}=[\mathbf{A}]\cdot[\mathbf{D}]\mathbf{u}, \tag{9}$$

where $[\mathbf{D}]$ is the differential operator and $[\mathbf{A}]$ the constitutive matrix built from the elastic characteristics of the material.

The linearity of the operator $[\mathbf{D}]$ permits one to obtain the (6×12) matrix $[\mathbf{h}(s,\omega)]$ and the six components vector $\mathbf{h}_0(s,\omega)$ connected to the unknown forces.

$$[\mathbf{h}(s,\omega)]=[\mathbf{D}][\mathbf{g}(s,\omega)],$$

$$\mathbf{h}_0(s,\omega)=[\mathbf{D}]\mathbf{g}_0(s,\omega).$$

Then the internal force vector is

$$\mathbf{f}(s,\omega)=[\mathbf{A}][\mathbf{h}(s,\omega)]\mathbf{c}+[\mathbf{A}]\mathbf{h}_0(s,\omega), \tag{10}$$

and the nodal force vector is

$$\begin{pmatrix}\mathbf{F}_A\\ \mathbf{F}_B\end{pmatrix}=\begin{pmatrix}-[\mathbf{A}]\,[\mathbf{h}(0,\omega)]\\ [\mathbf{A}]\,[\mathbf{h}(L,\omega)]\end{pmatrix}\mathbf{c}+\begin{pmatrix}-[\mathbf{A}]\mathbf{h}_0(0,\omega)\\ [\mathbf{A}]\mathbf{h}_0(L,\omega)\end{pmatrix}. \tag{11}$$

Internal force fields along the beam are evaluated from the nodal displacement vector $\mathbf{U}=(\mathbf{U}_A,\mathbf{U}_B)^{\mathrm{T}}$. This leads to the following solution

$$\mathbf{f}(s,\omega)=[\mathbf{A}][\mathbf{h}(s,\omega)]\begin{pmatrix}[\mathbf{g}(0,\omega)]\\ [\mathbf{g}(L,\omega)]\end{pmatrix}^{-1}\begin{pmatrix}\mathbf{U}_A-\mathbf{g}_0(0,\omega)\\ \mathbf{U}_B-\mathbf{g}_0(L,\omega)\end{pmatrix}+[\mathbf{A}]\mathbf{h}_0(s,\omega). \tag{12}$$

The dynamic stiffness matrix $[\mathbf{K}(\omega)]$ and the complementary force vector $\mathbf{P}(\omega)$ that is due to distributed loads are evaluated from the following definition

$$\begin{pmatrix} \mathbf{F}_A \\ \mathbf{F}_B \end{pmatrix} = [\mathbf{K}(\omega)] \begin{pmatrix} \mathbf{U}_A \\ \mathbf{U}_B \end{pmatrix} + \mathbf{P}(\omega). \tag{13}$$

Using Eqs. (7) and (11)

$$\begin{pmatrix} \mathbf{F}_A \\ \mathbf{F}_B \end{pmatrix} = \begin{pmatrix} -[\mathbf{A}][\mathbf{h}(0,\ \omega)] \\ [\mathbf{A}][\mathbf{h}(L,\ \omega)] \end{pmatrix} \begin{pmatrix} [\mathbf{g}(0,\ \omega)] \\ [\mathbf{g}(L,\ \omega)] \end{pmatrix}^{-1} \begin{pmatrix} \mathbf{U}_A - \mathbf{g}_0(0,\ \omega) \\ \mathbf{U}_B - \mathbf{g}_0(L,\ \omega) \end{pmatrix} + \begin{pmatrix} -[\mathbf{A}]\mathbf{h}_0(0,\ \omega) \\ [\mathbf{A}]\mathbf{h}_0(L,\ \omega) \end{pmatrix}$$

and then

$$[\mathbf{K}(\omega)] = \begin{pmatrix} -[\mathbf{A}][\mathbf{h}(0,\ \omega)] \\ [\mathbf{A}][\mathbf{h}(L,\ \omega)] \end{pmatrix} \begin{pmatrix} [\mathbf{g}(0,\ \omega)] \\ [\mathbf{g}(L,\ \omega)] \end{pmatrix}^{-1}, \tag{14}$$

$$\mathbf{P}(\omega) = \begin{pmatrix} [\mathbf{A}][\mathbf{h}(0,\ \omega)] \\ -[\mathbf{A}][\mathbf{h}(L,\ \omega)] \end{pmatrix} \begin{pmatrix} [\mathbf{g}(0,\ \omega)] \\ [\mathbf{g}(L,\ \omega)] \end{pmatrix}^{-1} \begin{pmatrix} \mathbf{g}_0(0,\ \omega) \\ \mathbf{g}_0(L,\ \omega) \end{pmatrix} + \begin{pmatrix} -[\mathbf{A}]\mathbf{h}_0(0,\ \omega) \\ [\mathbf{A}]\mathbf{h}_0(L,\ \omega) \end{pmatrix}. \tag{15}$$

2.3. Numerical continuous element (NCE) and dynamic transfer matrix

In many situations, couplings between displacement components (torsion, bending, extension and cross-section warping) occur. This contributes to raise the degree of the differential equations and inevitably, the search for closed form expressions of the dynamic responses becomes intractable if not impossible.

This method is not based on discretization of differential equations. The solution is exact but purely numerical as apposed to the close form solutions using characteristic functions which are applicable only in the simple case where uncoupling of vibration modes is possible.

2.3.1. State vector and elementary dynamic transfer matrix

The main idea is to use a vector variable composed of as many components as necessary to reduce the order of differential problem to one. In the case of a planar or non-planar Timoshenko/Saint-Venant beam, it has been shown that the vector, composed with both displacement and force components, satisfies first-order differential system relative to s, see Eq. (3). This vector is called the state vector $\mathbf{E}$:

$$\mathbf{E}_\omega(s) = (\mathbf{u}(s),\ \mathbf{f}(s))^t. \tag{16}$$

The vector $\mathbf{E}$ depends on the curvilinear co-ordinate, s and on the circular frequency ω indicated by a subscript. $\mathbf{u}(s)$ and $\mathbf{f}(s)$ are displacement and internal force vectors, respectively. In the case of harmonic regimes, the formulation of the elementary problem is written using this state vector

$$\frac{\mathrm{d}\mathbf{E}_\omega(s)}{\mathrm{d}s} = [\mathbf{D}_\omega(s)]\mathbf{E}_\omega(s), \tag{17}$$

where $[\mathbf{D}_\omega(s)]$ is the differential dynamic matrix.

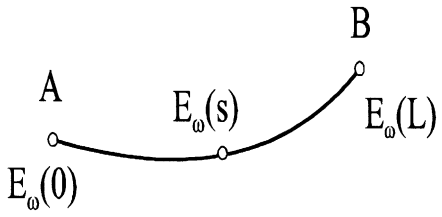

Fig. 3. State vector along the beam.

A dynamic transfer matrix is defined relating the state vector at the abscissa s to the input state vector at the origin of a beam segment, see Fig. 3

$$\mathbf{E}_\omega(s) = [\mathbf{T}_\omega(s)]_e \mathbf{E}_\omega(0). \tag{18}$$

According to Eqs. (17) and (18), a first order differential equation relates the dynamic transfer matrix and its first derivative to $[\mathbf{D}_\omega(s)]$

$$\frac{\mathrm{d}[\mathbf{T}_\omega(s)]}{\mathrm{d}s} = [\mathbf{D}_\omega(s)][\mathbf{T}_\omega(s)], \tag{19}$$

with $[\mathbf{T}_\omega(0)] = [\mathbf{I}]$ where $[\mathbf{I}]$ is the identity matrix.

If the differential matrix is supposed to be independent of the abscissa s, one gets the following first order differential equation

$$\frac{\mathrm{d}[\mathbf{T}_\omega(s)]}{\mathrm{d}s} = [\mathbf{D}_\omega][\mathbf{T}_\omega(s)]. \tag{20}$$

The beams which satisfy this assumption are those whose section, material and curvature/tortuosity radii are constant along the middle line. The most general case is the helical beam with constant section.

Matrix exponentials are introduced as solution of Eq. (20) for transfer matrix.

$$[\mathbf{T}_\omega(s)] = \mathrm{e}^{[\mathbf{D}_\omega]s}. \tag{21}$$

Exponential matrix is given by

$$\mathrm{e}^{[\mathbf{X}]} = \sum_{i=0}^{+\infty} \frac{[\mathbf{X}]^i}{i!}. \tag{22}$$

In the case where $[\mathbf{D}]$ is diagonalizable, the following decomposition is adopted

$$[\mathbf{D}_\omega]s = [\mathbf{Q}][\Lambda][\mathbf{Q}]^{-1}s, \tag{23}$$

where $[\mathbf{Q}]$ is the matrix whose columns are eigenvectors of $[\mathbf{D}_\omega]$ and $[\Lambda]$ the eigenvalues diagonal matrix $[\mathbf{D}_\omega]$.

Then expressions (21) and (22) allows one to obtain the following expression:

$$[\mathbf{T}_\omega(s)]s = [\mathbf{Q}]\mathrm{e}^{[\Lambda]s}[\mathbf{Q}]^{-1}, \tag{24}$$

with

$$e^{[\Lambda]} = \begin{pmatrix} e^{\lambda_1} & & & 0 \\ & e^{\lambda_2} & & \\ & & \ddots & \\ 0 & & & e^{\lambda_n} \end{pmatrix}. \tag{25}$$

If $[\mathbf{D}_\omega]$ cannot be diagonalized, it is possible to envisage a solution by a method using canonical Jordan form.

It is not possible to go further in the simplification of expression (23), $[\mathbf{D}_\omega]$ being neither a hermitian matrix nor a symmetrical one. Eigenvectors consequently are not orthogonal and the inversion of $[\mathbf{Q}_\omega]$ matrix is required.

2.3.2. Eigenvalues and eigenvectors of $[\boldsymbol{D}_\omega]$

The first step of the computation is the search for the eigenvalues. A QR, algorithm is used which permits one to obtain a complex set of eigenvalues of a real or complex matrix. For each operation a QR decomposition is effected by matrix multiplication

$$[\mathbf{A_k}] = [\mathbf{Q_k}][\mathbf{R_k}],$$
$$[\mathbf{A_{k+1}}] = [\mathbf{R_k}][\mathbf{Q_k}].$$

Successive operations lead to a triangular matrix whose diagonal elements are the required eigenvalues. The sensitivity of the eigenvalues to round-off errors can be reduced if a balancing of non-symmetric matrix is achieved beforehand.

The eigenvectors of $[\mathbf{D}_\omega]$ can be evaluated by matrix deflation or subspace iteration method.

2.3.3. Elementary dynamic stiffness matrix $[K_\omega]$

The elementary dynamic transfer matrix is defined as

$$\begin{pmatrix} \mathbf{U}_B \\ \mathbf{f}_B \end{pmatrix} = [\mathbf{T}(\omega)] \begin{pmatrix} \mathbf{U}_A \\ \mathbf{f}_A \end{pmatrix}, \tag{26}$$

that is to say

$$[\mathbf{T}(\omega)] = [\mathbf{T}_\omega(L)]. \tag{27}$$

A and B being the ends of the element and the dynamic stiffness matrix is defined from

$$\begin{pmatrix} \mathbf{F}_A \\ \mathbf{F}_B \end{pmatrix} = \begin{pmatrix} -\mathbf{f}_A \\ \mathbf{f}_B \end{pmatrix} = [\mathbf{K}(\omega)] \begin{pmatrix} \mathbf{U}_A \\ \mathbf{U}_B \end{pmatrix}, \tag{28}$$

where $\mathbf{F}_A$, $\mathbf{F}_B$, $\mathbf{U}_A$, $\mathbf{U}_B$ are external force vectors and generalized displacement vectors at both ends A and B. Decomposing $[\mathbf{T}_\omega]$ into four blocks and writing boundary conditions, the classical form of $[\mathbf{K}_\omega]$ is obtained

$$[\mathbf{K}(\omega)] = \begin{pmatrix} [\mathbf{T}_{12}(\omega)]^{-1}[\mathbf{T}_{11}(\omega)] & -[\mathbf{T}_{12}(\omega)]^{-1} \\ -[\mathbf{T}_{12}(\omega)]^{-\mathrm{T}} & [\mathbf{T}_{22}(\omega)][\mathbf{T}_{11}(\omega)]^{-1} \end{pmatrix}. \tag{29}$$

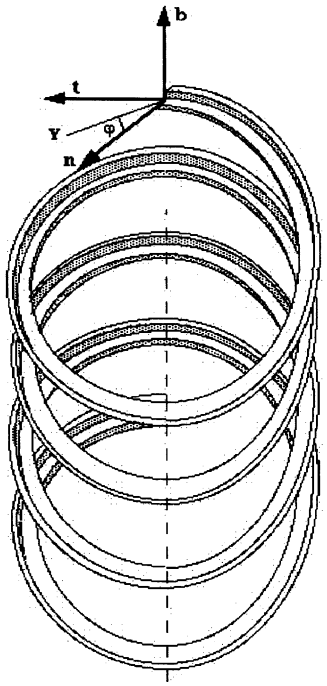

Fig. 4. Helical beam.

2.4. Helical Timoshenko beam

The geometry of this beam is interesting first by its extensive use in industry, see Fig. 4. (**t**, **n**, **b**) are the Frenet unit vectors, Y is the first direction of section inertia and ρ is the angle between vector **n** and Y.

From the computational point of view, it deserves attention because its dynamic response can be treated using a purely numerical method. This is due to the fact that curvature radius R of beam, tortuosity curvature T and section S are constant.

The state vector for the numerical continuous element formulation has 12 components (Expression (30))

$$\mathbf{E}_{\omega}(s) = (\mathbf{U}_r, \mathbf{U}_n, \mathbf{U}_b, \Omega_t, \Omega_n, \Omega_b, \mathbf{F}_t, \mathbf{F}_n, \mathbf{F}_b, \mathbf{M}_t, \mathbf{M}_n, \mathbf{M}_b). \tag{30}$$

The first three components concern displacement. The second group of three components is an angular rotation. The third group of three components concerns force components. The fourth group represents moment components. Non-dimensional variables are used,

$$\bar{s} = \frac{s}{R}, \ \bar{U} = \frac{U}{R}, \ \bar{\Omega} = \Omega, \ \bar{F} = \frac{FR^2}{EI_Y}, \ \bar{M} = \frac{MR}{EI_Y},$$

where E is Young's modulus and I_Y is the area moment of inertia with respect to Y-axis.

Differential dynamic transfer matrix $[\mathbf{D}_{\omega}]$, which is defined from a first order differential equation, is presented in Appendix A.

2.5. Solution and post-processing

The harmonic response of a complete structure is studied in a given frequency range. For each circular frequency, each elementary dynamic stiffness matrix is built and converted from local reference to global reference, according to expression (31).

$$[\bar{\mathbf{K}}(\omega)] = [\mathbf{R}]_e^{\mathrm{T}}[\mathbf{K}(\omega)][\mathbf{R}]_e, \tag{31}$$

where $[\mathbf{R}]_e$ is the rotating matrix from a local reference to a global reference.

The assembling of all these stiffness matrices and the introduction of boundary condition are operated to conduct to the global dynamic stiffness $[\mathbf{K}(\omega)]_G$.

This constitutes a linear system whose unknowns are displacements of the beam at its tips (Eq. (32)):

$$\mathbf{F}_G + \mathbf{P}_G = [\mathbf{K}(\omega)]_G \mathbf{U}_G, \tag{32}$$

where $[\mathbf{K}(\omega)]_G$ is the global dynamic stiffness matrix.

Displacement and internal forces along the beams are evaluated from nodal solutions according to Eqs. (8) and (12), in the case of explicit continuous element and, according to Eq. (18), in the case of numerical ones.

2.6. Numerical instability for numerical continuous element

For numerical continuous elements, it will be shown that numerical instability may occur particularly for the elementary theory. This instability occurs beyond a critical frequency that can be predicted in advance.

Take a simple example: the Bernoulli–Euler beam for bending dynamic differential matrix is easily evaluated;

$$[\mathbf{D}_\omega] = \begin{pmatrix} 0 & 1 & 0 & 0 \\ 0 & 0 & 0 & 1 \\ -\dfrac{\rho S L^4 \omega^2}{EI_Z} & 0 & 0 & 0 \\ 0 & 0 & -1 & 0 \end{pmatrix}. \tag{33}$$

The associate state vector is

$$\mathbf{E}_\omega = (U_Y(s),\ \Omega_Z(s),\ F_Y(s),\ M_Z(s))^{\mathrm{T}},$$

where the components are those defined previously, see Eq. (3).

Matrix (33) has four distinct non-zero eigenvalues,

$$\lambda_1 = \mathrm{j}m_\omega,\ \lambda_2 = -\mathrm{j}m_\omega,\ \lambda_3 = m_\omega,\ \lambda_4 = -m_\omega$$

with

$$m_\omega = L\sqrt[4]{\frac{\rho S\omega^2}{EI_Z}}.$$

Matrix (33) is used to implement a numerical continuous element according to Section 2.3.

The dynamic stiffness matrix (34) has a close form expression. It is used to implement an explicit continuous element.

$$[\mathbf{K}_\omega]_e = \frac{m_\omega}{(1-cC)} \begin{pmatrix} m_\omega^2(Cs+Sc) & m_\omega sS & -m_\omega^2(s+S) & m_\omega(C-c) \\ m_\omega sS & (Cs-Sc) & m_\omega(c-C) & (S-s) \\ -m_\omega^2(s+S) & m_\omega(C-c) & m_\omega^2(Sc+Cs) & -m_\omega sS \\ m_\omega(C-c) & (S-s) & -m_\omega sS & (sC-Sc) \end{pmatrix}, \tag{34}$$

where C=cosh(m_ω), c=cos(m_ω), S=sinh(m_ω) and s=sin(m_ω).

Fig. 5 shows the flexural responses using ECE and NCE. Beyond 30 000 Hz, there is a complete loss of accuracy with NCE due to round-off errors.

The numerical values of hyperbolic functions C and S exceed 10^{15} in the transfer matrix. Although exponential evolution is continuous, loss of information occurs when each term of the dynamic transfer matrix necessitates, for its representation, a number exceeding 16 figures.

For the Bernoulli–Euler beam, the inversion of $[\mathbf{T}_{12}(\omega)]$, in expression (29), necessitates the presence of all the decimal figures.

When m_ω>38, the submatrix $[\mathbf{T}_{12}(\omega)]$ becomes numerically

$$[\mathbf{T}_{12}(\omega)] \cong \begin{pmatrix} -m_\omega^{-3} & m_\omega^{-2} \\ -m_\omega^{-2} & m_\omega^{-1} \end{pmatrix} \frac{e^{m_\omega}}{2},$$

and then it is not possible to invert it.

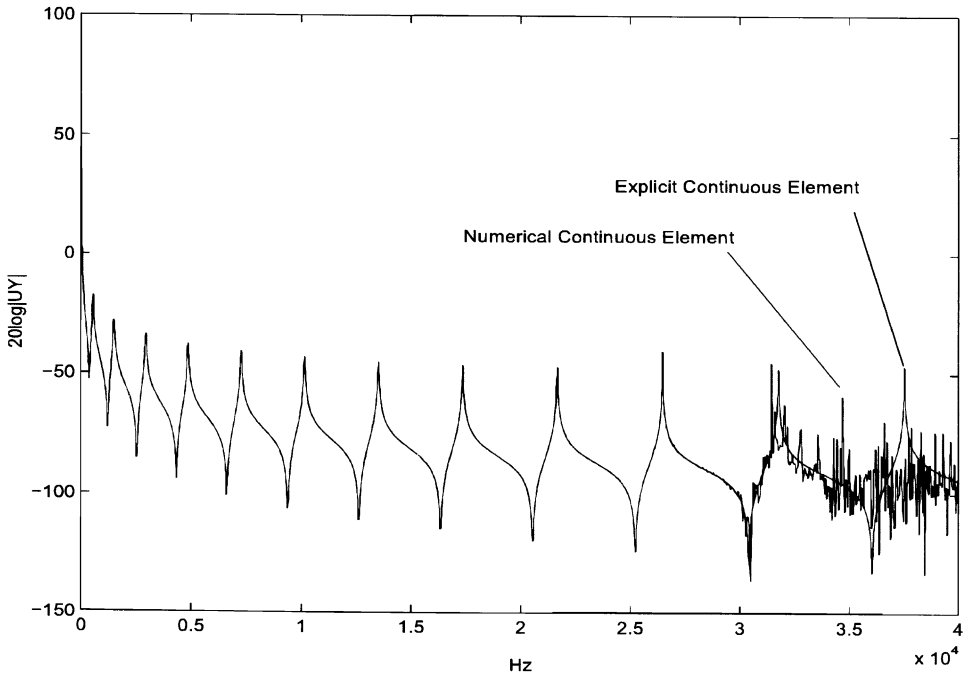

Fig. 5. Numerical instability.

When $20 < m_\omega < 38$, the inversion is theoretically possible but very hazardous from the numerical point of view. The instability occurs.

This limit for m_ω gives rise to the critical frequency:

$$f = \frac{400}{2\pi L^2}\sqrt{\frac{EI_Z}{\rho S}}.$$

For the chosen example, it is situated at 30 000 Hz.

3. Validation tests

Three tools are used: continuous elements, finite elements and physical experiments.

3.1. Numerical validation tests

3.1.1. Timoshenko beam theory

Although close form expressions can be evaluated for transfer and stiffness matrices [11], a numerical continuous element is used to evaluate its performances.

Instability in the response curve does not occur because the hyperbolic terms in submatrix $[\mathbf{T}_{12}(\omega)]$ become trigonometric beyond a critical frequency. This submatrix is then numerically invertible.

The upper bound of the frequency interval, for the same beam geometry as in Bernoulli–Euler beam, is situated beyond 3×10^9 Hz. This value is the frequency limit of the numerical procedure relating to a single element model. It does not presume the validity of the Timoshenko beam theory at such frequencies.

Fig. 6 shows the bending response of a straight beam whose characteristics are:

$$L = 0.7\,\text{m}, \quad S = 3 \times 10^{-3}\,m^2, \quad I_Y = 6.25 \times 10^{-7}\,m^4, \quad k_Y = 1.2,$$
$$E = 210\,000\,\text{MPa}, \quad G = 80\,769\,\text{MPa}, \quad \rho = 7800\,kg/m^3,$$

where L is the length of the beam and the other characteristics have been defined previously.

The results obtained with one numerical continuous element are compared with those obtained with 16, 32 and 64 beam finite elements.

There is a convergence of results obtained with NCE and FE up to 60 000 Hz. Beyond this limit, there is a discrepancy which can be explained by the fact that the meshing in FE idealization is not fine enough.

3.1.2. Timoshenko–Saint-Venant beam theory

Fig. 7 shows the state variables of the coupled system represented by the beam with an U-shaped cross-section. If the shear centre C does not coincide with inertia centre G, coupling phenomena between bending and torsion appear.

In Appendix B the dynamic differential matrix is presented. This matrix involves the position (y_C, z_C) of the shear centre in the plane of the cross-section.

Fig. 8 shows an example of the response curve obtained by such a computation. A beam with an L-shaped cross-section is submitted to a transverse force that gives rise to a coupled torsion/

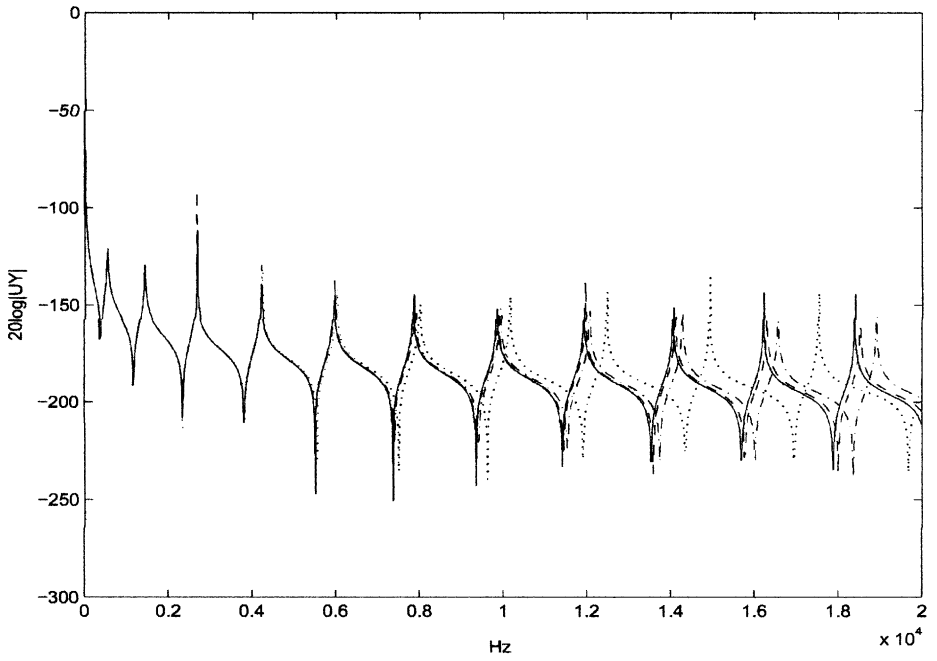

Fig. 6. Comparison NCE/FE. —, 1 NCE; … 16 FE; -.-., 32 FE; - - -, 64 FE.

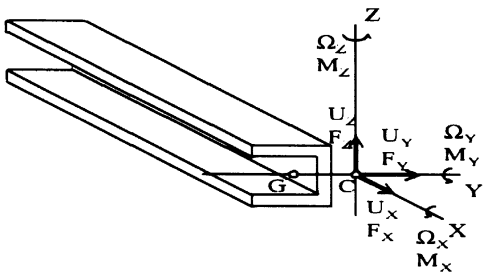

Fig. 7. Coupled bending/torsion state variables.

bending motion. The models compared are built, respectively, with one NCE and 80 shell finite elements. The characteristics of the beam are:

$$L = 1.003\,\text{m}, \quad S = 1.71 \times 10^{-4}\,\text{m}, \quad I_Y = 2.32 \times 10^{-8}\,\text{m}^4,$$
$$I_Z = 5.94 \times 10^{-9}\,\text{m}^4, \quad J = 5.13 \times 10^{-10}\,\text{m}^4, \quad y_c = 0.01\,\text{m},$$
$$z_C = 0\,\text{m}, \quad k_Y = k_Z = 2.79,$$
$$E = 208\,560\,\text{MPa}, \quad G = 80\,215\,\text{MPa}, \quad \rho = 7800\,\text{kg/m}^3,$$

where J is the torsional constant, the other characteristics have been defined previously.

A good similarity can be noticed between the two curves. Furthermore, the numerical continuous element has given a stable response over a large frequency range. The numerical

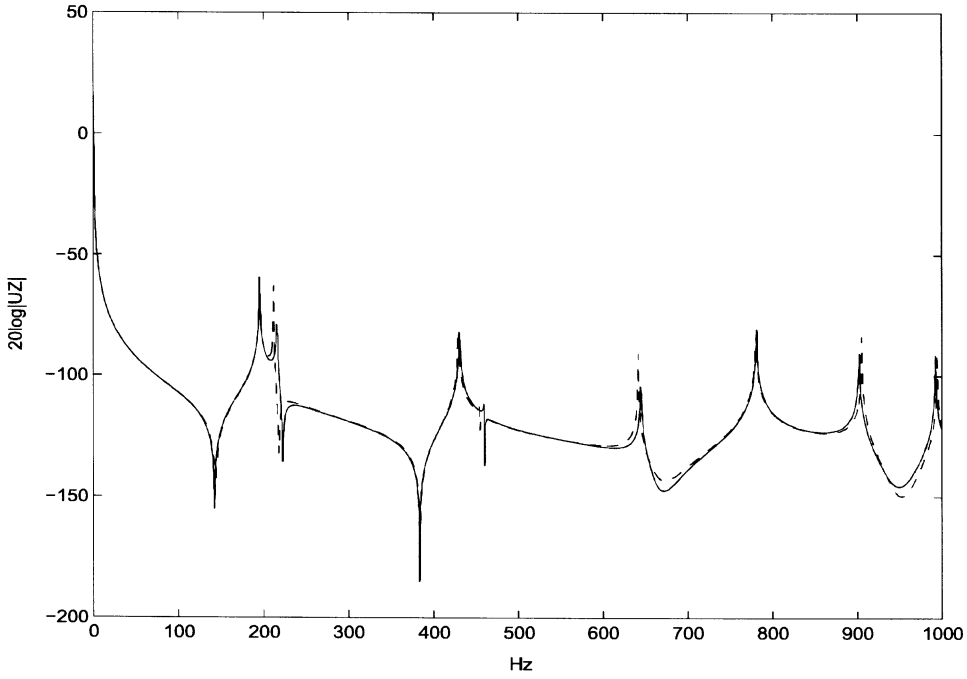

Fig. 8. Comparison 1 NCE/80 shell FE —: CE, - - -: FE.

frequency limit relating to a single element model has been evaluated to about 10^8 Hz, far beyond the frequency range of validity for this beam theory.

3.1.3. Timoshenko–Vlasov beam theory

The Vlasov torsion theory is more elaborated than Saint-Venant torsion theory. The presence of a clamped end creates non-constant warping along the beam and normal stresses which are particularly important for an open profile. This theory introduces the bimoment, that is, the seventh generalized force directly proportional to the derivatives of the cross-section rotation in its plane. Fig. 9 represents the cross-section of the clamped–free beam submitted to computation. Its characteristics are:

$$L = 0.7\,\text{m}, \quad a = 3.3 \times 10^{-2}\,\text{m}, \quad b = 3 \times 10^{-2}\,\text{m}, \quad e = 3 \times 10^{-3}\,\text{m},$$
$$E = 210\,000\,\text{MPa}, \quad v = 0.3, \quad \rho = 7800\,\text{kg/m}^3.$$

The state vector has 14 components. The equations of motion and the differential dynamic matrix are evaluated [16]. The beam is submitted to a torsion moment at the free tip and the displacement response is evaluated at this tip. Fig. 10 shows calculations using one NCE (Saint-Venant and Vlasov) and 60 shell finite elements. It shows that the Saint-Venant's formulation gives rise rapidly to a degradation of results in response.

The numerical frequency limit relating to a single element model has been evaluated beyond 15 000 Hz. Larger frequencies could be reached with models composed of 2 or more elements.

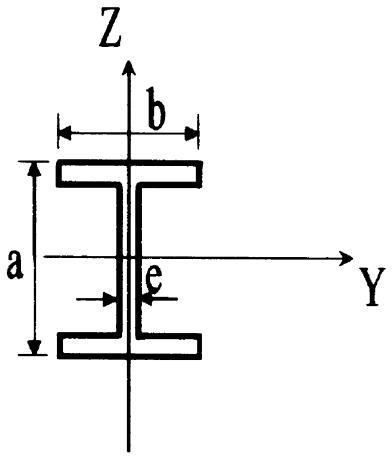

Fig. 9. Cross-section of the element tested.

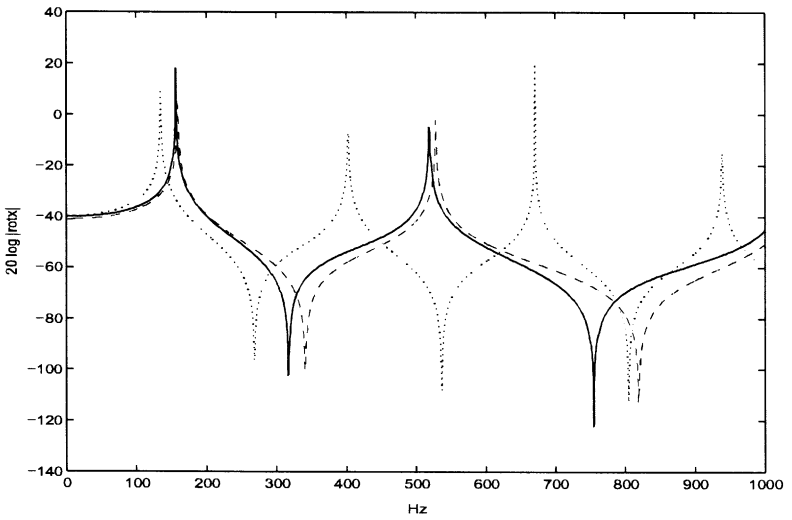

Fig. 10. Comparison Saint-Venant/Vlasov ECN and Shell FE: — 1 Vlasov NCE, … 1, Saint-Venant NCE, - - -, 120 shell FE.

3.1.4. Helical beam

Fig. 11 shows the helical spring tested. Its geometrical characteristics are:

$$S = 8.825 \times 10^{-5}\,\mathrm{m}^2, \quad k_Y = k_Z = 1.11, \quad I_Y = I_Z = 6.197 \times 10^{-10}\,\mathrm{m}^4,$$
$$J = I_0 = 1.239 \times 10^{-9}\,\mathrm{m}^4,$$
$$R = 0.06973\,\mathrm{m}, \quad T = 0.3591\,\mathrm{m}, \quad L = 1.72\,\mathrm{m}, \quad \varphi = 0\,\mathrm{rad}.$$

These characteristics have been defined in Section 2.4.

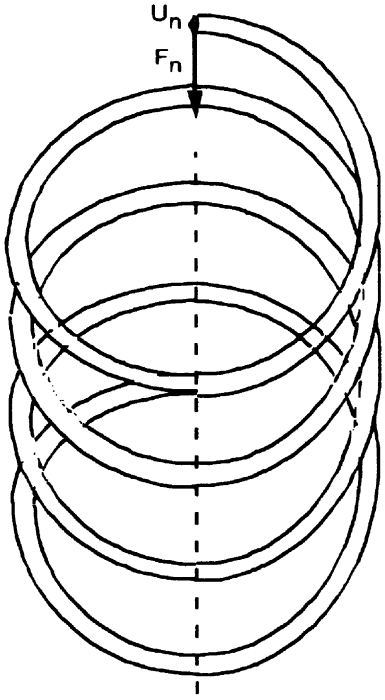

Fig. 11. Helical beam.

The differential dynamic matrix is presented in Appendix A. Although many turns of coil are present, one continuous element is only used. Fifty and 100 elements are adopted in the FE models. In Fig. 12, excellent convergence is noticed for CE and FE with 100 elements.

3.1.5. *Computation of damped structures*

The dynamic stiffness matrix can include complex terms due to structural damping. No hypothesis is made on the nature of damping. If constitutive equations of materials are known, introduction of complex modulii (Young's and Coulomb modulii as $E^* = E_0(1+j\delta_E)$, $G^* = G_0(1+j\delta_G)$ is easy and the differential dynamic matrix $[\mathbf{D}_\omega]$ is specified with complex components. Furthermore, complex modulii may be frequency dependent. Fig. 13 shows an example of such computation. It is the response of the helical beam presented in the previous subsection for several values of the factor $\delta=\delta_E=\delta_{Gg}$. The responses are evaluated for the frequency range [250, 500 Hz].

3.2. *Physical experiments*

The experimental set-up is used for structural modal analysis, see Fig. 14. The beams tested are submitted to a shock for a free–free boundary condition. The response is treated by a spectral analyzer.

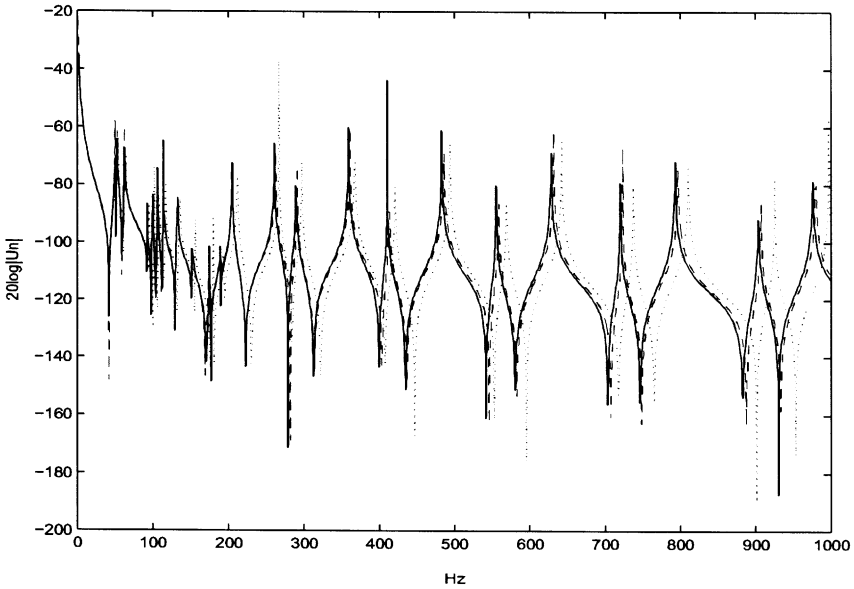

Fig. 12. Comparison 1 NCE/50 FE/100 FE: —, 1 NCE, …, 50 beam FE; - - -, 100 beam FE.

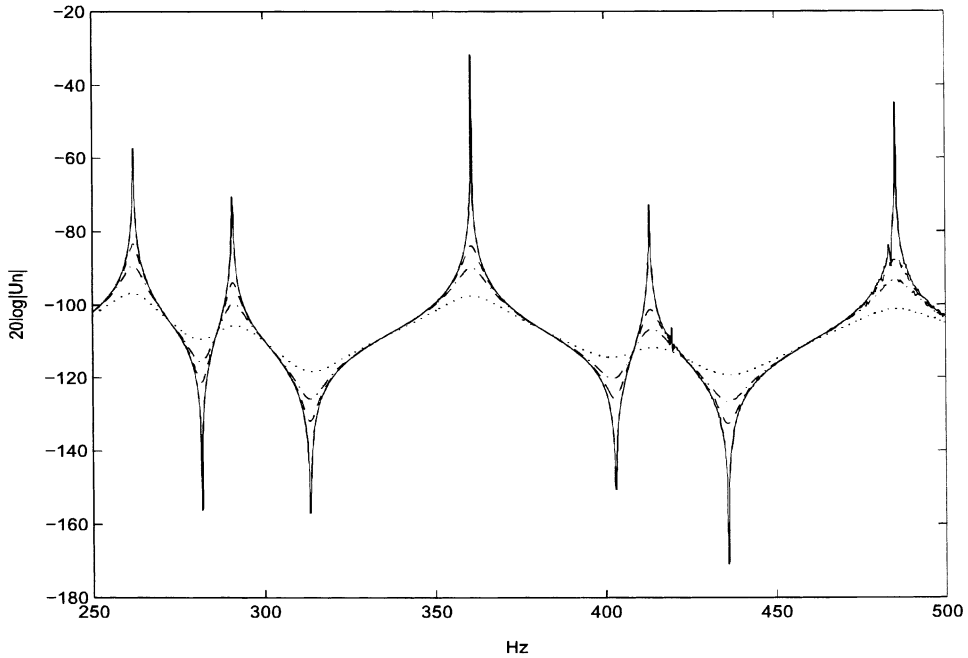

Fig. 13. Dynamic response of a damped helical beam: —, $\delta = 0$; - - -, $\delta = 0.01$; -.-., $\delta = 0.02$; …, $\delta = 0.05$.

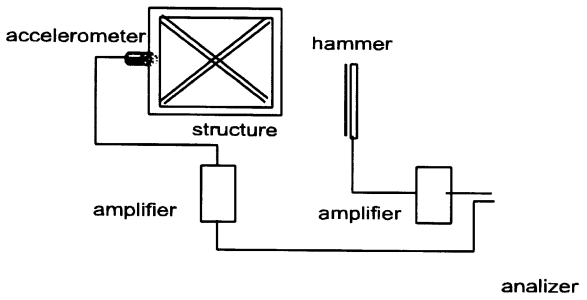

Fig. 14. Experimental set-up.

Table 1
Comparison of first 19 eigenfrequencies

Mode	Bernoulli	Rayleigh	Timoshenko	Cowper	Tests
1	31	31	31	31	31
2	87	87	87	87	87
3	170	170	170	170	170
4	281	281	281	281	281
5	420 (0.2%)	420	418	418	419
6	587 (0.5%)	586	583	583	584
7	782 (0.9%)	780	775	775	775
8	1004 (1%)	1001	993	993	994
9	1254 (1.4%)	1249	1237	1237	1237
10	1532 (1.5%)	1524	1507 (0.1%)	1507	1509
11	1838 (1.4%)	1827	1801 (0.6%)	1802	1812
12	2171 (2.1%)	2157	2121 (0.2%)	2122	2125
13	2532 (2.3%)	2513	2465 (0.4%)	2465	2475
14	2921 (2.9%)	2896	2832 (0.2%)	2833	2837
15	3338 (3.1%)	3305	3222 (0.5%)	3224	3237
16	3783 (3.6%)	3740	3635 (0.4%)	3637	3650
17	4255 (4.1%)	4202	4070 (0.4%)	4072	4087
18	4755 (4.5%)	4690	4526 (0.5%)	4529	4550
19	5283 (5.1%)	5203	5003 (0.4%)	5007	5025

3.2.1. *Timoshenko's bending beam*

In Table 1, only 19 eigenvalues among the first 34 eigenvalues up to 150 00 Hz are mentioned. Various theories of bending are used in the CE computations. Compared to physical experiments, the accuracy of a Timoshenko beam is about 0.5%. Less elaborated theories of bending (Bernoulli, Rayleigh) give rise to larger discrepancies reaching 15%.

3.2.2. *Helical Timoshenko's beam*

Table 2 shows some first 20 eigenvalues. Only one continuous element is used. The discrepancies between computation and test results are 2.5% for the first 72 eigenvalues.

Table 2
First 20 eigenfreguencies obtained by NCE and tests

Mode	NCE	Tests	Mode	NCE	Tests
1	52	52	11	179 (3%)	185
2	54 (3.5%)	56	12	181 (3.5%)	188
3	64 (3%)	66	13	195 (2%)	199
4	95 (3%)	98	14	210 (4%)	219
5	103	103	15	268 (2.5%)	275
6	109 (2%)	111	16	268 (2.5%)	275
7	117 (1.5%)	119	17	369 (2.5%)	379
8	125 (3%)	129	18	422 (3.5%)	437
9	136 (3.5%)	141	19	496 (2.5%)	509
10	156 (3%)	161	20	570 (3.5%)	591

4. Concluding remarks

The continuous element method is very efficient to solve vibration problems of complex beam assemblies. It is specially suited to the problem of harmonic response of large structures. The number of elements required is reduced to a minimum and the obtained solution is theoretically exact. The formulation based on close form expressions of the elementary problem is limited to straight beam assemblies. The numerical continuous element method is an easy way to extend the applications of the formulation, then the vibration problem concerning assemblies including more complex beam geometries is soluble. Furthermore, the solutions obtained are capable of describing various effects (inertia, shear, warping, couplings, etc.) which influence the structure responses. Explicit or numerical formulations cover in principle an infinity of eigenvalues. In practice for a given frequency interval, the structural response can be evaluated by a frequency scanning method.

Acknowledgements

The authors wish to acknowledge the French Army Research Offices for the financial support which permit the creation of the Continuous Element Code ETAPE and the preparation of the first author's thesis.

Appendix A

Helical beam differential dynamic matrix

$$[\mathbf{D}_\omega] = \begin{pmatrix} [\mathbf{D}_{11}] & [\mathbf{D}_{12}] \\ [\mathbf{D}_{21}] & [\mathbf{D}_{22}] \end{pmatrix},$$

$$[\mathbf{D}_{11}] = \begin{pmatrix} 0 & 1 & 0 & 0 & 0 & 0 \\ -1 & 0 & \frac{R}{T} & 0 & 0 & 1 \\ 0 & -\frac{R}{T} & 0 & 0 & -1 & 0 \\ 0 & 0 & 0 & 0 & 1 & 0 \\ 0 & 0 & 0 & -1 & 0 & \frac{R}{T} \\ 0 & 0 & 0 & 0 & -\frac{R}{T} & 0 \end{pmatrix},$$

$$[\mathbf{D}_{12}] = \begin{pmatrix} \frac{I_Y}{SR^2} & 0 & 0 & 0 & 0 & 0 \\ 0 & \frac{EI_Y}{GSR^2}(k_Y\cos^2\varphi + k_z\sin^2\varphi) & \frac{EI_Y}{GSR^2}(k_Y - k_Z)\cos\varphi\sin\varphi & 0 & 0 & 0 \\ 0 & \frac{EI_Y}{GSR^2}(k_Y - k_Z)\cos\varphi\sin\varphi & \frac{EI_Y}{GSR^2}(k_Y\sin^2\varphi + k_z\cos^2\varphi) & 0 & 0 & 0 \\ 0 & 0 & 0 & \frac{EI_Y}{GJ} & 0 & 0 \\ 0 & 0 & 0 & 0 & \cos^2\varphi + \frac{I_Y}{I_Z}\sin^2\varphi & \cos\varphi\sin\varphi\left(1 - \frac{I_Y}{I_Z}\right) \\ 0 & 0 & 0 & 0 & \cos\varphi\sin\varphi\left(1 - \frac{I_Y}{I_Z}\right) & \sin^2\varphi + \frac{I_Y}{I_Z}\cos^2\varphi \end{pmatrix},$$

$$[\mathbf{D}_{21}] = \begin{pmatrix} -\frac{\rho SR^4\omega^2}{EI_Y} & 0 & 0 & 0 & 0 & 0 \\ 0 & -\frac{\rho SR^4\omega^2}{EI_Y} & 0 & 0 & 0 & 0 \\ 0 & 0 & -\frac{\rho SR^4\omega^2}{EI_Y} & 0 & 0 & 0 \\ 0 & 0 & 0 & -\frac{\rho I_0R^2\omega^2}{EI_Y} & 0 & 0 \\ 0 & 0 & 0 & 0 & -\frac{\rho R^4\omega^2}{EI_Y}\left(\cos^2\varphi + \frac{I_Z}{I_Y}\sin^2\varphi\right) & 0 \\ 0 & 0 & 0 & 0 & 0 & -\frac{\rho R^4\omega^2}{EI_Y}\left(\sin^2\varphi + \frac{I_Z}{I_Y}\cos^2\varphi\right) \end{pmatrix},$$

$$[\mathbf{D}_{22}] = \begin{bmatrix} 0 & 1 & 0 & 0 & 0 & 0 \\ -1 & 0 & \frac{R}{T} & 0 & 0 & 0 \\ 0 & -\frac{R}{T} & 0 & 0 & 0 & 0 \\ 0 & 0 & 0 & 0 & 1 & 0 \\ 0 & 0 & 1 & -1 & 0 & \frac{R}{T} \\ 0 & -1 & 0 & 0 & -\frac{R}{T} & 0 \end{bmatrix}.$$

Appendix B

Coupled bending/torsion differential dynamic matrix for a straight beam

$$[\mathbf{D}_\omega] = \begin{pmatrix}
0 & 0 & 0 & 0 & 1 & \frac{k_Y EI_Y}{GSL^2} & 0 & 0 & 0 & 0 \\
0 & 0 & 0 & -1 & 0 & 0 & \frac{k_Y EI_Y}{GSL^2} & 0 & 0 & 0 \\
0 & 0 & 0 & 0 & 0 & 0 & 0 & \frac{EI_Y}{GJ} & 0 & 0 \\
0 & 0 & 0 & 0 & 0 & 0 & 0 & 0 & 1 & 0 \\
0 & 0 & 0 & 0 & 0 & 0 & 0 & 0 & 0 & \frac{I_Y}{I_Z} \\
-\frac{\rho SL^4\omega^2}{EI_Y} & 0 & -zC\frac{\rho SL^3\omega^2}{EI_Y} & 0 & 0 & 0 & 0 & 0 & 0 & 0 \\
0 & -\frac{\rho SL^2\omega^2}{EI_Y} & y_C\frac{\rho SL}{EI_Y} & 0 & 0 & 0 & 0 & 0 & 0 & 0 \\
-z_C\frac{\rho SL^3\omega^2}{EI_Y} & y_C\frac{\rho SL^3\omega^2}{EI_Y} & -\frac{\rho L^2\omega^2}{EI_Y}(I_0 + y_C^2 S + z_C^2 S) & 0 & 0 & 0 & 0 & 0 & 0 & 0 \\
0 & 0 & 0 & -\frac{\rho L^2\omega^2}{E} & 0 & 0 & 1 & 0 & 0 & 0 \\
0 & 0 & 0 & 0 & \frac{\rho L^2 I_Z\omega^2}{EI_Y} & -1 & 0 & 0 & 0 & 0
\end{pmatrix}$$

References

[1] R. Lunden, B. Akesson, Damped second order Rayleigh Timoshenko beam vibration in space — an exact complex dynamic member stiffness matrix, International Journal for Numerical Methods in Engineering 19 (1983) 431–449.

[2] C. Duforêt, Dynamic study of an assembling of rods in medium and higher frequency ranges—Computer code ETAPE, in: Proceedings of the Third Colloquiium on New Trends in Structure Calculations, Bastia, Corsica, 1985, pp. 229–246 (in French).

[3] M.S. Anderson, F.W. Williams, J.R. Banerjee, B.J. Durling, C.L. Herstorm, D. Kennedy, D.B. Warnaar, User Manual for BUNVIS-RG: an exact buckling and vibration program for lattice structures, with repetitive geometry and substructuring options, NASA Technical Memorandum 87669, 1986.

[4] F.W. Williams, D. Kennedy, R. Butler, M.S. Anderson, VICONOPT: program for exact vibration and buckling analysis or design of prismatic plate assemblies, American Institute of Aernautics and Astronautics Journal 29 (1991) 1927–1928.

[5] P.H. Kulla, Continuous elements, some practical examples. In: Proceedings of the ESTEC Workshop on Continuum Methods for Flexible Structures, Noordwÿk, The Netherlands, June 1989.

[6] T.H. Richards, Y.T. Leung, An accurate method in vibration analysis, Journal of Sound and Vibration 55 (3) (1977) 363–376.

[7] A.Y.T. Leung, Dynamic Stiffness and Substructures, Springer, New York, 1993.

[8] D.J. Gorman, A high accurate analytical solution for free vibration analysis of simply supported right rectangular plates, Journal of Sound and Vibration 89 (1983) 107–118.

[9] V. Kolousek, Dynamics in Engineering Structures, Butterworths, London, 1973.

[10] R.W. Clough, J. Penzien, Dynamic of Structures, McGraw-Hill, New York, 1975.

[11] J.C. Snowdon, Vibration and Shock in Damped Mechanical Systems, Wiley, New York, 1968.

[12] S. Kevorkian, M. Pascal, An accurate method for free vibration analysis of structures with application to plates, Journal of Sound and Vibration 246 (5) (2001) 795–814.

[13] J.R. Banerjee, Coupled bending-torsional dynamic stiffness matrix for beam elements, International Journal for Numerical Methods in Engineering 28 (1989) 1283–1289.
[14] C. Duforêt, H. Grangier, J.P. Quintin, Corrélation calculs-mesures de la dynamiquc d'une structure tubulaire jusquà des fréquences élevées, Proceedings of Strucome 88, vol. 2, Paris, 1988.
[15] W.H. Wittrick, F.W. Williams, A general algorithm for computing natural frequencies of elastic structures, The Quarterly Journal of Mechanics and Applied Mathematics 24 (1971) 263–284.
[16] J.B. Casimir, Beam Continuous Elements, Static and Dynamic Studies of Assemblies of Planar and Non-planar Beams, Thesis, ISMCM, Department of Structure and Rheology, Saint-Ouen, 1997 (in French.)